Open Access Journal
Journal of Power Technologies 94 (Nuclear Issue) (2014) 51–60
journal homepage:papers.itc.pw.edu.pl

Impact of local property variations of reactor coolant on cladding temperature distribution in supercritical water reactors

Jianguo Zhong, Steven P. Antal, Michael Z. Podowski*
Center for Multiphase Research, Rensselaer Polytechnic Institute, USA

Abstract

Fluids at supercritical pressures are considered to be very promising as coolants for Generation IV reactor systems, including the supercritical water cooled reactor (SCWR), the CO_2-cooled reactor (SCCO2R) and the Brayton cycle as a secondary system in sodium-cooled fast reactors.

The operating conditions of such reactors allow for a significant thermodynamic efficiency increase of the respective power plants. On the other hand, several unresolved issues must still be addressed in order to develop a viable design of supercritical fluid nuclear systems. Examples include: in-core heat transfer in SCWRs, heat exchangers in the S-CO2 Brayton cycle, and flows in complex geometries of SCO2 compressors.

It has been shown before that the understanding of the effect of fluid property variations on turbulence is a major factor in our ability to predict the combined fluid mechanics and heat convection in systems and components using supercritical fluids. The objective of this paper is to present the results of analysis on the effect of local multidimensional flow and heat transfer phenomena on the temperature distribution inside future SCWRs. Two proposed SCWR designs have been considered: a single-pass and a two-pass coolant flow configurations through the reactor core.

It should be noted that a preliminary documentation of the results of the current work has been included in the materials of the NURETH-15 conference.

Keywords: Local property variations of reactor coolant, Reactor coolant, Cladding temperature distribution, Supercritical water reactors

1. Introduction

One of the major tasks associated with developing next generation nuclear power plants is achieving significantly higher efficiency of the thermodynamic cycle than is possible in current generation reactors. This paper looks at the supercritical water-cooled reactor (SCWR), which is a promising Gen. IV reactor. Since no phase change occurs in the core at coolant pressures above the critical pressure, a direct energy conversion cycle can be used, which in turn considerably simplifies the overall plant and component design. Furthermore, no in-vessel recirculation pumps or jet pumps are needed, thus improving the safety characteristics of the reactor pressure vessel.

The focus of the present work is on two design concepts of future SCWRs. One is the single-pass coolant flow configuration, the other is the two-pass flow arrangement. Both design concepts are summa-

*Corresponding author
Email address: podowm@rpi.edu (Michael Z. Podowski*)

rized in the next section.

1.1. Reactor Fuel Design

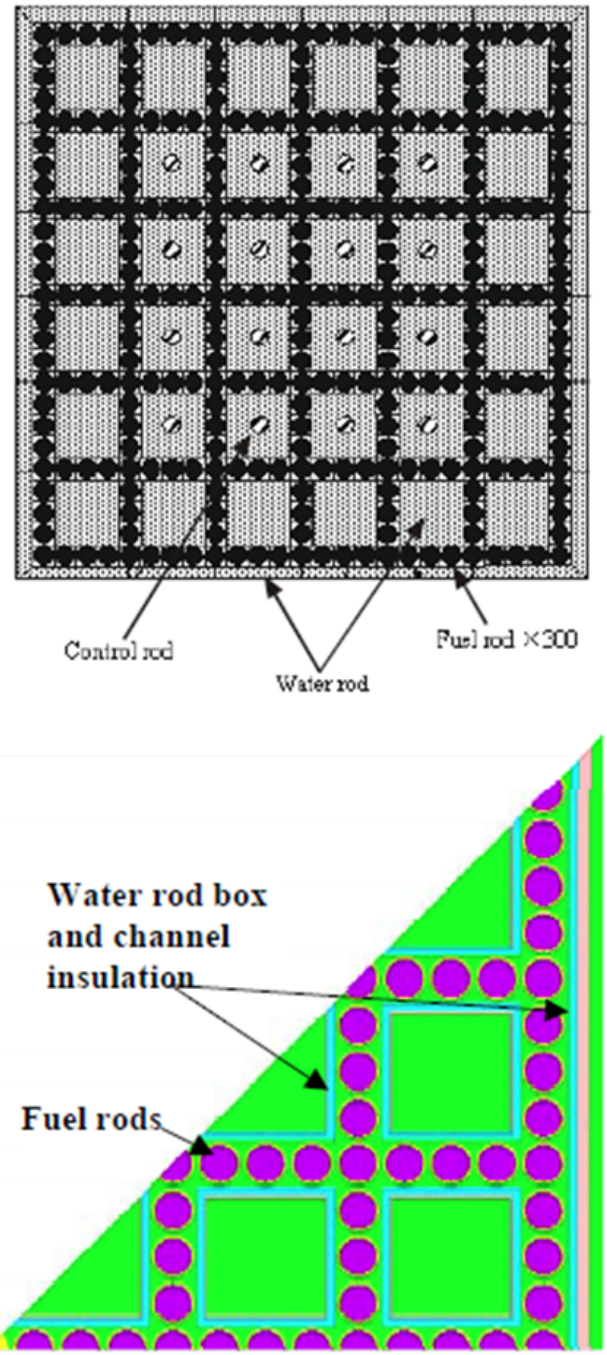

Figure 1: Square SCWR fuel assembly design [1]

Fig. 1 shows one of the proposed designs of the SCWR fuel assemblies [1]. The assembly consists of multiple cylindrical fuel pins and the surrounding coolant channels, and square water boxes (or rods) located in a regular square array. The presence of water rods helps to achieve a more uniform coolant/moderator density distribution inside the core, thus mitigating the effect of the sharply decreasing density of the water removing heat from the fuel elements along the coolant channels.

Table 1: Reference reactor fuel assembly design for U.S. generation-IV SCWR [1]

Number of fuel pins per assembly	300
Number of water rod per assembly	36
Water rod side, mm	33.6
Number of control rod fingers per assembly	16
Assembly side, mm	280
Fuel pin diameter, mm	10.2
Fuel pin pitch, mm	11.2
Heated length, m	4.87

Typical dimensions of the assembly shown in Fig. 1 are given in Table 1.

1.2. One-Pass Flow Arrangement

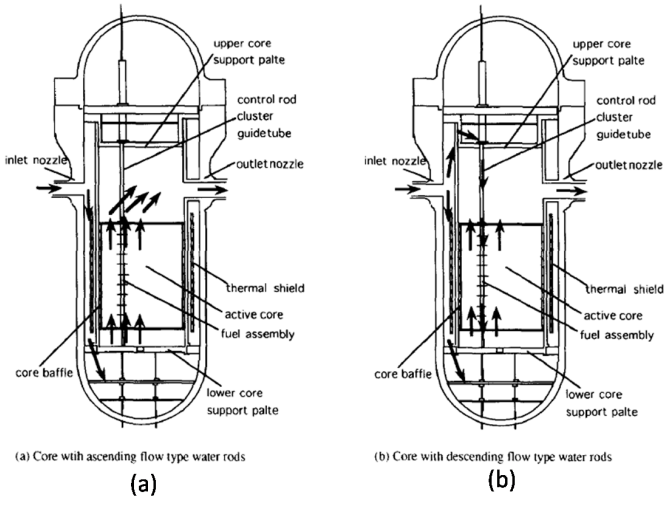

Figure 2: Scheme of one-pass and two-pass reactor designs [2]: (a) single-pass flow path, (b) two-pass flow path

In the conventional PWR reactor design, the coolant flow from the inlet nozzles is guided into the lower plenum and enters the core from the bottom. This is shown in Fig. 2(a). As the coolant flows upward, it removes the heat from fuel elements and then enters the upper plenum and leaves the reactor pressure

vessel through the outlet nozzles. The advantage of the one-pass flow arrangement is its simple geometry. Such an approach can also be used in SCWRs by dividing the flow at the bottom of the core between the coolant channels and water rods. Since the heat transfer rate from the coolant channels to the water rods is a small fraction of the reactor power, the flow through the water rods would be very low compared to that through the coolant channels. Thus, the water inside the square water boxes would mainly serve as a neutron moderator.

1.3. Two-Pass Flow Arrangement

Another flow path design is shown in Fig. 2(b). In this case, the coolant flow is divided into two paths, one entering the core from the top and flowing downward, the other flowing downward along the downcomer outside the core and mixing with the other part of the flow in the lower plenum. As a result, the total amount of coolant flows through the coolant channels and removes the heat from the fuel. The supercritical water temperature at the inlet to the coolant channels is slightly higher than at the inlet to the reactor pressure vessel, while at the same time the total heating rate between the inlet and outlet of the channels is diminished by the heat transfer into the water rods. Naturally, the coolant outlet temperature at the top of the core is the same in both cases. On the other hand, the combined effects of mixing at the bottom of the core and heating the water inside the water rods depend on factors such as the local effective heat transfer coefficient between the main flow and the water rod flow and the axial power distribution along the fuel elements.

2. Model description

Two models were used in the present analysis: a one-dimensional (1-D) model and a multidimensional (3-D) CFD model. Both models are described in this section.

The two models were compared against each other to assess the impact of 1-D modeling assumptions on the predicted wall heat transfer. Based on the comparative analysis, the 1-D model was subsequently modified and used to evaluate the maximum cladding temperature for both the single-pass and two-pass SCWR designs.

2.1. One-Dimensional Coolant Flow Model

According to a 1-D modeling framework, the conservation energy equation along a fuel-assembly-averaged coolant channel can be written as

$$\frac{dh_{as}}{dz} = \frac{q'_{as}(z)}{w_{as}} \tag{1}$$

where $h_{as}(z)$ is the local coolant enthalpy, w_{as} is the mass flowrate per single assembly, and q'_{as} is the linear heat rate along the average assembly.

Whereas the actual axial power profile along reactor fuel elements at various stages of reactor operation is obtained from the coupled neutronics/thermal-hydraulics model, a standard generic power distribution was deemed appropriate in the present analysis, given by

$$q'_{as}(z) = q'_{as,o} \sin\left(\pi \frac{z}{L}\right) \tag{2}$$

where L is the active length of fuel elements.

If Eq. (2) is applied to the average fuel assembly, the maximum linear heat rate at the center of the assembly is determined from

$$q'^{av}_{as,o} = \frac{P_R}{N_{as}L} F_H \tag{3}$$

where P_R is the reactor power, N_{as} is the total number of fuel assemblies in the core, and $F_H \approx \pi/2$ is the axial peaking factor.

Naturally, Eq. (2) can be applied to the hot assembly. In this case, we have

$$q'^{hot}_{as,o} = q'^{av}_{as,o} F_R = \frac{P_R}{N_{as}L} F_H F_R \tag{4}$$

Eq. (1) can be integrated along the channel length to obtain the axial distribution of the coolant bulk enthalpy for any given fuel assembly, $h_b(z)$. The corresponding coolant bulk temperature is obtained from

$$T_b(z) = T\left(h_b(z),\, p_{sys}\right) \tag{5}$$

where p_{sys} is the coolant operating pressure.

In the case of a two-pass core design, 1-D energy conservation equations are used for both the coolant channels and the water 'rods', and they are respectively given by

$$\frac{dh^{ch}_{as}}{dz} = \frac{1}{w_{as}} \left[q'^{fuel}_{as}(z) - q'^{ch-wr}_{as}(z)\right] \tag{6}$$

$$\frac{dh_{as}^{wr}}{dz} = \frac{1}{w_{as}^{wr}} q_{as}^{\prime ch-wr} \tag{7}$$

where $q_{as}^{\prime ch-wr}(z)$ is the local linear rate of heat transfer between the coolant channels and water rods, and $w_{as}^{wr} = \eta w_{as}$ is the water flowrate per assembly along the water rods.

The linear heat transfer rate between the coolant channel and water rods can be expressed as

$$q_{as}^{\prime ch-wr}(z) = P_H H_{eff} \left[T_{as}^{ch}(z) - T_{as}^{wr}(z) \right] \tag{8}$$

where P_H is the heated perimeter and H_{eff} is the effective heat transfer coefficient given by

$$\frac{1}{H_{eff}} = \frac{1}{H_{as}^{ch}} + \frac{1}{H_{as}^{wr}} \tag{9}$$

In Eq. (9), H_{as}^{ch} and H_{as}^{wr} are the heat transfer coefficients at the coolant channel and water-rod sides, respectively, of the water rod walls.

The coupled Eq. (6) and Eq. (7) are solved with the following boundary conditions:

$$At\ core\ top: \qquad h_{as}^{wr} = h_{in} \tag{10}$$

$$At\ core\ bottom: \quad h_{as,in}^{ch} = \eta h_{as,ex}^{wr} + (1-\eta) h_{in} \tag{11}$$

2.2. One-Dimensional Coolant Heat Convection

The determination of the heat transfer coefficient in fluids at supercritical pressures is difficult due to the dramatic property variations in the pseudo-critical temperature region. As shown in Fig. 3, the thermal conductivity, dynamic viscosity and density of water significantly decrease in this region, while the specific heat experiences a sharp narrow spike.

Several correlations have been developed to date, aimed at capturing the impact of property variations on the average heat transfer coefficient. An illustration of the predictive capabilities of such correlations is shown in Fig. 4.

As can be seen, no single correlation is capable of predicting the results of measurements for different experimental conditions. Since the Dittus-Boelter correlation is the most commonly used one for a variety of applications, it was chosen as a basic reference in the current 1-D model. Its applicability was tested by comparing the predictions against those of a complete multidimensional model.

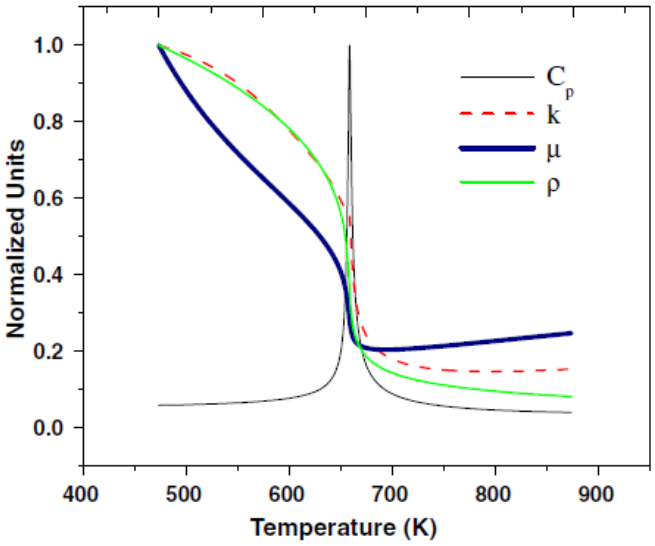

Figure 3: Normalized thermophysical property variation of water in the pseudo-critical region at 25 MPa [3]

2.3. Multidimensional CFD Model

Local phenomena of combined flow and heat transfer in both single-phase and multiphase/multicomponent fluids can be modeled using a multidimensional modeling framework. A general form of the fluid conservation equations for mass, energy and momentum can be written as [6]

$$\frac{\partial \rho}{\partial t} + \nabla \cdot \left(\rho \underline{v} \right) = 0 \tag{12}$$

$$\frac{\partial \left(\rho \underline{v} \right)}{\partial t} + \nabla \cdot \left(\rho \underline{v} \underline{v} \right) = -\nabla p + \nabla \cdot \underline{\underline{\tau}}^{tot} + \rho \underline{g} \tag{13}$$

$$\frac{\partial (\rho h)}{\partial t} + \nabla \cdot \left(\rho \underline{v} h \right) = -\nabla \cdot \underline{q}^{\prime\prime tot} + \frac{Dp}{Dt} + \rho \underline{g} \underline{v} \tag{14}$$

where $\underline{\underline{\tau}}^{tot} = \underline{\underline{\tau}}^{turb} + \underline{\underline{\tau}}^{\prime\prime\prime}$ is the combined turbulent (Reynolds) and molecular shear stress, $\underline{\underline{q}}^{\prime\prime tot} = \underline{\underline{q}}^{\prime\prime turb} + \underline{\underline{q}}^{\prime\prime m}$ is the combined turbulent and molecular heat flux, and the remaining notation is conventional.

Among the models for the turbulent (Reynolds) stress, $\underline{\underline{\tau}}^{turb}$, that have been developed so far for CFD simulations, the most commonly used one is the $k-\varepsilon$

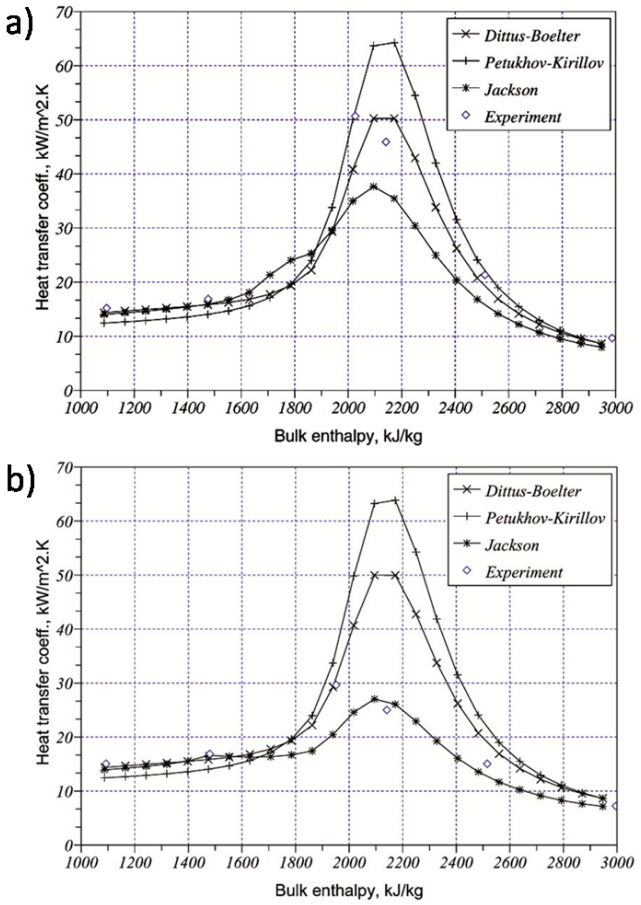

Figure 4: A comparison [4] between the heat transfer coefficients in a 10 mm diameter vertical pipe, measured by Yamagata et al. [5] and predicted by various correlations. The operating conditions are: system pressure, $p = 24.5$ MPa; coolant mass flux, $G = 1200$ kg/m^{2}s, wall heat flux: (a) $q'' = 465$ kW/m^2, (b) $q'' = 930$ kW/m^2

model and its High-Reynolds-Number (HRN) and Low-Reynolds Number (LRN) versions. For application to supercritical fluids, the standard $k-\varepsilon$ model was reformulated to express all state variables using the Favre averaging concept. Specifically, the transport equations for the turbulent kinetic energy, k, and the energy dissipation rate, ε, respectively, were formulated as

$$\frac{\partial(\rho k)}{\partial t} + \nabla \cdot \left(\rho \underline{v} k\right) = \nabla \cdot \left[\left(\mu + \frac{\mu_t}{Pr}\right) \nabla k\right] + P + G - \rho\varepsilon - D \tag{15}$$

$$\frac{\partial(\rho \varepsilon)}{\partial t} + \nabla \cdot \left(\rho \underline{v} \varepsilon\right) = \nabla \cdot \left[\left(\mu + \frac{\mu_t}{Pr}\right) \nabla \varepsilon\right] + C_1 f_2 \frac{\varepsilon}{k} (P + G) - C_2 \rho \frac{\varepsilon}{k} + E \tag{16}$$

where the fluid physical properties, including the density, ρ, and the molecular viscosity, μ, present the Favre-averaged quantities, the eddy viscosity is calculated as, $\mu_t = C_\mu f_\mu \rho \frac{k^2}{\varepsilon}$, D and E account for local near-wall phenomena in the LRN model (and are both zero in the HRN model), and f_μ and f_2 are the LRN damping constants in the boundary layer region (they become unity in the HRN case).

Whereas this model typically (although not without exceptions) yields reasonable results for constant property fluids, its application to supercritical fluids, especially near the pseudo-critical temperature where fluid properties undergo dramatic changes, requires careful analysis. Details of the computational model used in the present case were documented by Gallaway et al. [6, 7]. In particular, the heated wall temperature is given by

$$T_w = T_p + \frac{q''}{u^* \rho c_{p,m}} \left[Pr_m^{\frac{2}{3}} y_{csl}^+ + \frac{Pr_t}{\kappa} \ln\left(\frac{y^+}{y_{csl}^+} Pr_m^{\frac{1}{3}}\right)\right] \tag{17}$$

where

$$Pr_m = (1-\zeta)\, Pr_P + \zeta Pr_w \tag{18}$$

$$c_{p,m} = (1-\zeta)\, c_{p,P} + \zeta c_{p,w} \tag{19}$$

and $0 \le \zeta \le 1$ is the weighting factor between the properties at the wall and at the grid point nearest the wall.

3. NPHASE-CMFD Code

NPHASE-CMFD [8] is a segregated and coupled, nominally pressure-based finite volume multiphase/multicomponent CFD code. The individual transport equations are solved for the: momentum, energy and turbulence quantities for each field. Both HRN and LRN $k-\varepsilon$ models were encoded in this code. The mixture and field continuity equations are solved in coupled or uncoupled fashions, using frozen coefficient linearizations. The code is fully unstructured and can utilize second-order accurate convection and diffusion discretizations.

All governing equations account for local pressure- and temperature-dependent fluid properties. The

properties of both supercritical water and supercritical carbon dioxide can be evaluated based on the analytical spline-type models which have been incorporated in NPHASE-CMFD [7].

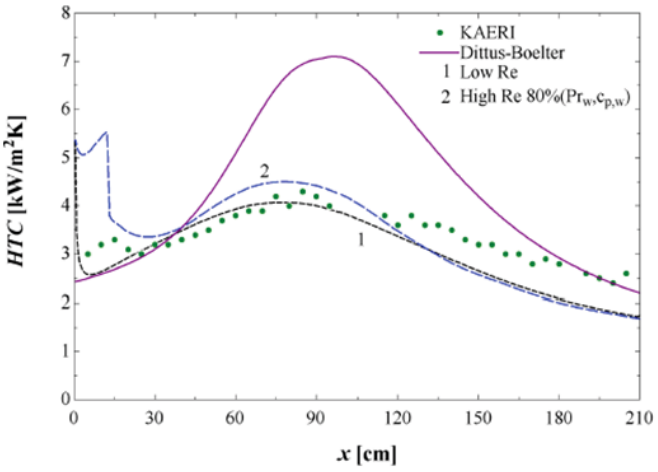

Figure 5: Heat transfer coefficient along a uniformly heated channel cooled using supercritical CO_2 [7]

An illustration of the predictive capabilities of the NPHASE-CMFD-based model for situations relevant to the present study is shown in Fig. 5.
As can be readily noticed, the near-wall fluid temperature depends not only on the properties at the near-wall grid point but also, and perhaps more heavily, on the properties between this grid point (p) and the wall (w). The quantitative impact of such local property variations can be directly assessed by varying the averaging factor in Eqs. (17)–(19). As shown in Fig. 5, the results for the LRN model are very close to those for the HRN model, using an 80/20 split between the properties at the wall and those at the near-wall location corresponding to $y+$ of about 40. The heat transfer coefficient predicted by both models agrees quite well with the experimental data of Kim et al. [9].

4. Results and analysis

Both the 1-D and 3-D models described in Section 2 were used in a comparative analysis for typical anticipated SCWR designs discussed in Section 1. The operating conditions used as a reference are shown in Table 2.
The first part of the analysis is concerned with the single-pass design. As was mentioned earlier, in such a case the flowrate through the water rods is expected to be very small compared to the flow rate inside the reactor coolant channels and, consequently, the heat transfer rate from the channels to the water rods is going to be practically negligible compared to the reactor fuel heating rate. Consequently, it can be assumed that the core power is entirely removed by the main flow inside the coolant channels.

Table 2: Reference reactor operating conditions of Gen-IV SCWR

Thermal power, GWt	3
Operating pressure, MPa	25
Reactor inlet temperature, °C	280, 300, 350
Reactor total flow rate, Mg/s	2
Number of fuel assemblies	145

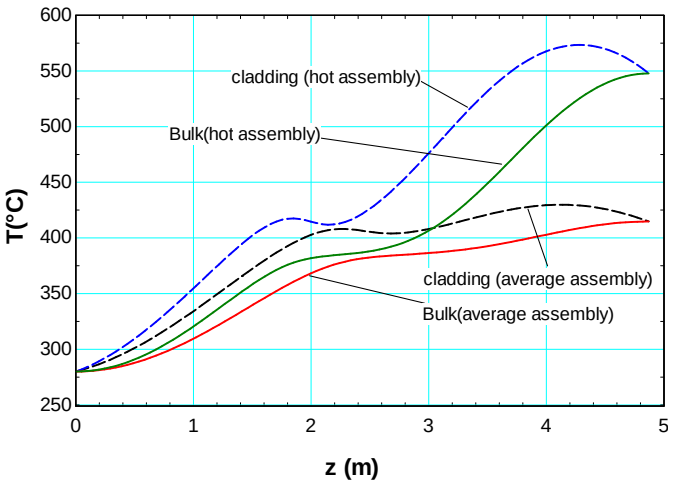

Figure 6: Axial coolant and cladding temperature distributions for the average and hot channels, corresponding to the inlet temperature, T_{in} = 280°C

The 1-D calculations were performed for the average reactor channel and the hot channel. In both cases, the Dittus-Boelter correlation was used for the axially-dependent heat transfer coefficient. The results for the inlet temperature of 280°C are shown in Fig. 6.
The core-average exit temperature of the coolant was 418°C, and the hot channel exit temperature was 550°C. It is interesting to notice that the 'hot channel'-to-'average channel' ratio of coolant temperature increase was 1.96, whereas the corresponding enthalpy ratio (equal to the radial peaking factor)

was 1.4. The maximum fuel element cladding surface temperature was 574°C, and it exceeded the hot channel exit temperature by only 24°C.

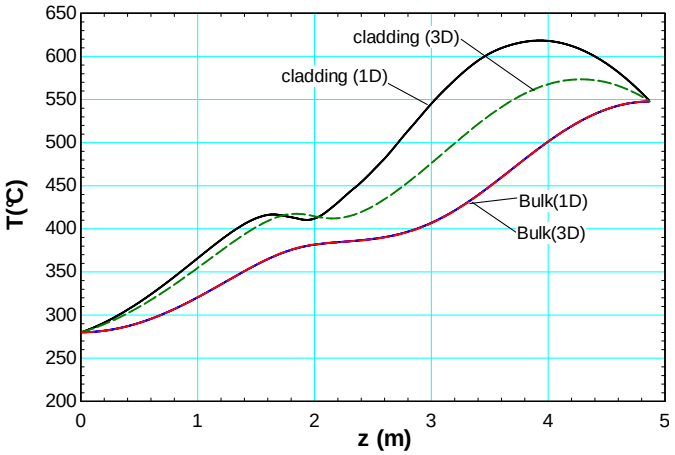

Figure 7: A comparison between the coolant and cladding axial temperature distributions along the hot fuel assembly, obtained using 3-D and 1-D models for coolant inlet temperature of 280°C

Next, calculations were performed using a multidimensional model encoded in NPASE-CMFD for the same reactor operating conditions. The results of the predictions for the hot channel are shown in Fig. 7, and they are compared against the 1-D results. As can be seen, the coolant bulk temperature obtained using the detailed CFD model agreed well with the 1-D calculations based on the basic energy balance. However, as expected, the cladding surface temperature distribution predicted by the NPHASE-CMFD-based model differs considerably from that obtained using the Dittus-Boelter 1-D correlation. This outcome is consistent with the results of the previous studies, such as those shown in Figures 4 and 5. The maximum cladding temperature predicted using the 3-D model exceeds that from the 1-D model by about 40°C.

An interesting aspect of the consequences of supercritical water property variation with temperature is their effect on average coolant velocity as it approaches the top of the core. The axial velocity distribution along the heated channel for the same conditions as used in Fig. 7 are shown in Fig. 8.

As can be seen, a dramatic density decrease results in a nearly ten-fold increase in coolant velocity between the core inlet and exit. It is also interesting to

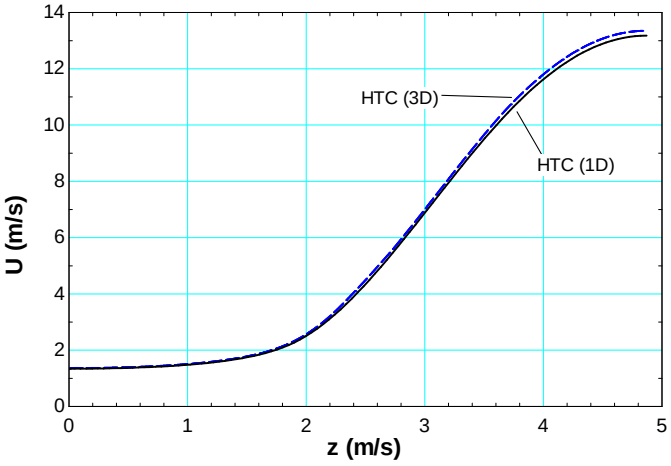

Figure 8: Axial distribution of the bulk coolant velocity along the hot assembly for the inlet temperature, T_{in} = 280°C

notice that whereas practically the same bulk temperature along the flow is predicted by the 1-D and 3-D models, the velocity calculated by the 3-D model increases a little faster than that obtained from the 1-D model. This is due to the fact that the former velocity accounts for the effect of lateral density distribution changes between the channel center and the heated wall.

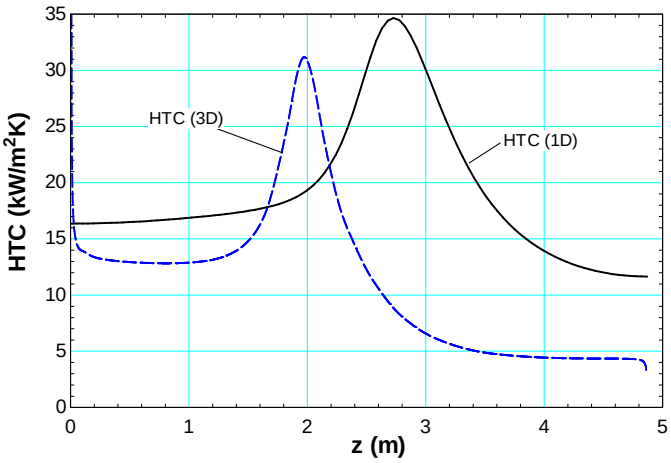

Figure 9: Axial distributions of the heat transfer coefficient along the hot channel, obtained from the 3-D and 1-D models with T_{in} = 280°C

Details behind the observed differences can be readily understood by examining the axial distributions of the heat transfer coefficients, one deduced from the 3-D simulations and the other obtained directly from the Dittus-Boelter correlation. As shown in Fig. 9, the relative distributions are qualitatively sim-

ilar to those in Fig. 5.

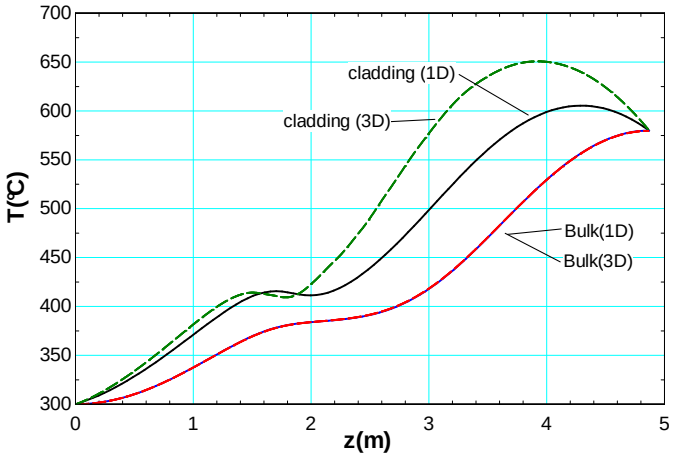

Figure 10: A comparison between the coolant and cladding axial temperature distributions along the hot fuel assembly, obtained using 3-D and 1-D models for coolant inlet temperature of 300°C

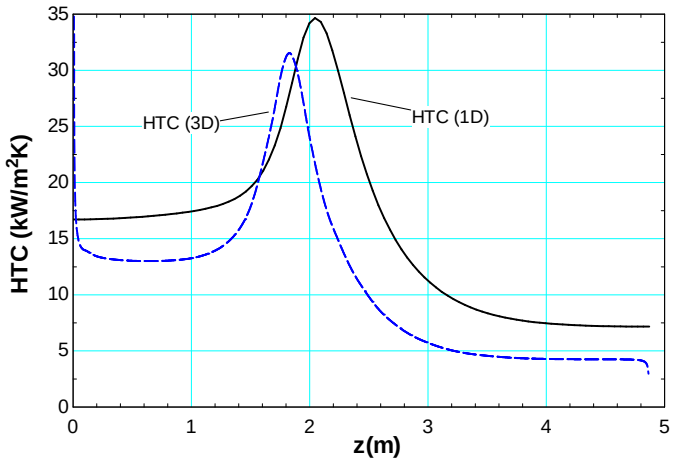

Figure 11: Axial distributions of the heat transfer coefficient along the hot channel, obtained from the 3-D and 1-D models with T_{in} = 300°C

As can be seen in Figures 10 through 13, similar trends have been observed for the inlet temperature of 300°C and 350°C. However, the rate at which the maximum cladding temperature increased was higher than the corresponding change in the inlet coolant temperature. Specifically, the increase in the inlet temperature by 20°C, from 280°C to 300°C, raised the maximum cladding surface temperature predicted by the 3-D model by about 30°C, whereas a further increase by 50°C, from 300°C to 350°C, caused a 110°C increase in the maximum

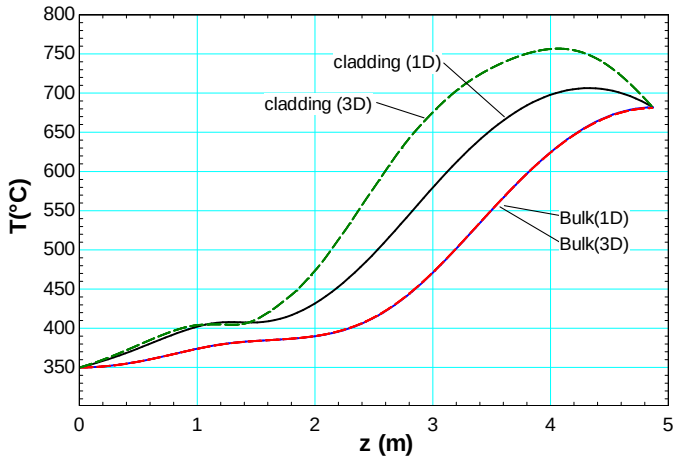

Figure 12: A comparison between the coolant and cladding axial temperature distributions along the hot fuel assembly, obtained using 3-D and 1-D models for coolant inlet temperature of 350°C

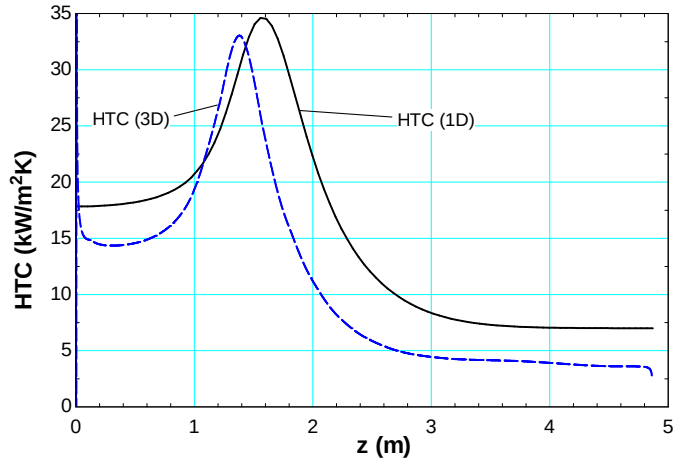

Figure 13: Axial distributions of the heat transfer coefficient along the hot channel, obtained from the 3-D and 1-D models with T_{in} = 350°C

cladding temperature. In all three cases, the maximum cladding temperature obtained from the 1-D model was lower by about 50°C than the corresponding 3-D prediction.

The comparison between 1-D and 3-D model predictions can conveniently be illustrated by examining the axial distributions of the ratio of the corresponding heat transfer coefficients. This is shown in Fig. 14. As can be seen, the observed trends are similar in all three cases. In particular, the value of the ratio around the location where the cladding temperature reaches a maximum is about 1.8.

As mentioned before, the results shown in Fig. 6

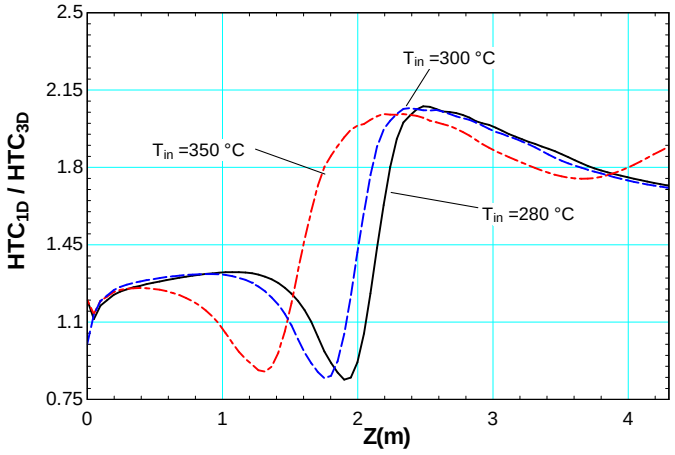

Figure 14: Axial distributions of the 1-D to 3-D heat transfer coefficient ratios in the hot channel for three different coolant inlet temperatures

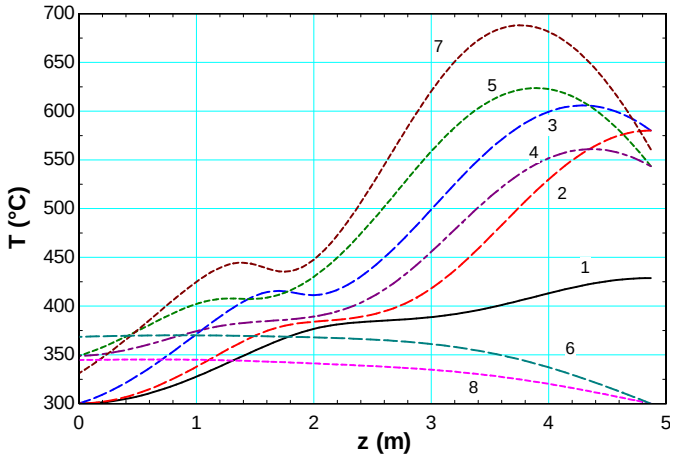

Figure 15: Axial temperature distributions along the SCWR core (from the bottom upward) for the coolant inlet temperature, T_{in} = 300°C: 1—coolant bulk temperature along the average channel (fuel assembly) for a single-pass case, 2—coolant bulk temperature along the hot channel (fuel assembly) for a single-pass case, 3—cladding temperature along the hot channel (fuel assembly) for a single-pass case, 4—coolant bulk temperature along the hot channel (fuel assembly) for a two-pass case, 5—cladding temperature along the hot channel (fuel assembly) for a two-pass case using the 1-D Dittus-Boelter correlation, 6—bulk temperature along the water rods for a two-pass case using the 1-D Dittus-Boelter correlation, 7—cladding temperature along the hot channel (fuel assembly) for a two-pass case using a modified heat transfer correlation consistent with the 3-D model predictions, 8—bulk temperature along the water rods for a two-pass case using a modified heat transfer correlation consistent with the 3-D model predictions

through Fig. 14 refer to a single-pass core design, assuming that the flowrate through the water rods is very small compared to the flow rate inside the coolant channels and the heat transfer rate from the channels to the water rods is negligible. To quantify the effect of downflow along the water rods in the case of a two-pass design, calculations were performed assuming that 10% of the total flowrate is initially directed into the water rods from the top of the core. During the flow toward the bottom of the core, the water gets slightly heated and then mixes in the lower plenum with the remaining 90% coolant, which is still at the inlet temperature. Then, the mixture enters the reactor coolant channels at the bottom of the core at a total flow rate and a slightly higher temperature.

The purpose of the analysis was to quantify the effect of the proposed two-pass design on the maximum cladding temperature. Typical results of calculations are shown in Fig. 15. They include a comparison between the single-pass and two-pass predictions, as well as between two models of fuel-to-coolant heat convection. Naturally, the exit bulk temperature is the same in all the cases analyzed. The effect of flow configuration was first investigated using the Dittus-Boelter correlation for the heat transfer coefficient. As can be seen, the maximum cladding temperature for the two-pass case (curve-5) is slightly higher than that for a single-pass (curve-3), although the difference is rather small (10°C or less). The corresponding bulk temperature along the hot-assembly water rods is plotted as curve-6. Whereas this temperature increases by over 80°C at the bottom of the core, for the current flow split the mixture temperature at the exit to the coolant channels increases only by about 10°C or less. Interestingly, the increase in the coolant bulk temperature at the inlet to the coolant channels between the two-pass and single-pass cases is very similar to the corresponding increase in the maximum cladding temperature. It is important to mention that this conclusion is valid for a wide range of flow splits in the two-pass configurations. For instance, for a 90% flow along the water rods, both temperature increases are of the order of 80°C.

Another series of calculations for a two-pass case were performed assuming that the heat transfer coefficient was reduced in a manner reflecting the impact of local multidimensional phenomena. The resultant cladding temperature distribution obtained for

the heat transfer equal to $1/1.8 = 0.56$ of the 1-D values is shown as curve-7 in Fig. 15. Comparing this result against a complete 3-D single-pass simulation shown in Fig. 6, one concludes that the maximum cladding temperature for the two-pass case is about 15°C higher than that for a single pass.

Two major conclusions can be drawn from the results shown in Fig. 15. Firstly, it important to realize that whereas the use of a two-pass design can reduce the coolant bulk temperature increase across the coolant channels by 10% to 20%, the corresponding maximum cladding temperature will experience a similar increase (in degrees). Secondly, the use of 1-D correlations for the heat transfer coefficient at supercritical pressures may significantly underestimate the maximum cladding temperature.

5. Conclusions

A parametric analysis of heat transfer and temperature distribution in the core of the proposed supercritical water reactor (SCWR) was performed. Two design concepts for coolant flow were investigated: single-pass and two-pass configurations. Computer simulations were performed using two models: a one-dimensional (1-D) model and a multidimensional CFD model. The validation results of the latter model are shown.

One of the major findings of the present work is that from the fluid flow and heat transfer perspective, the maximum cladding temperature increase between the two-pass and single-pass configurations is similar to the corresponding increase in the inlet temperature to coolant channels. Thus, the desired reduction in the coolant temperature increase along the coolant channels leads to a proportionally higher hot-spot cladding surface temperature. Another important conclusion is that using 1-D models may lead to underpredictions of the maximum cladding temperature and, thus, to nonconservative results. It is clear that future work should capitalize on the predictive capabilities of complete multidimensional models of coolant flow and heat transfer. Furthermore, such simulations should be coupled with a multidimensional model of core neutronics. This in turn should lead to the development of improved reactor designs aimed at mitigating the effect of variable properties of supercritical water on the local nonuniform temperature distributions across the reactor core [10].

Acknowledgments

The authors wish to acknowledge the financial support provided to this study by the NEUP Program of the U.S. Department of Energy.

References

[1] P. MacDonald, J. Buongiorno, J. W. Sterbentz, C. Davis, R. Witt, Feasibility study of supercritical water cooled reactors for electric power production, Final Report INEEL/EXT-04-02530, Idaho National Laboratory (INL) (2005).

[2] Y. Oka, S. Koshizuka, T. Yamasaki, Direct cycle light water reactor operating at supercritical pressure, J. Nucl. Sci. Technol 29 (1992) 585–588.

[3] J. Licht, M. Anderson, M. Corradini, Heat transfer to water at supercritical pressures in a circular and square annular flow geometry, Int. J. Heat Fluid Flow 29 (2008) 156–166. doi:10.1016/j.ijheatfluidflow.2007.09.007.

[4] H. Anglart, T. Gallaway, S. P. Antal, M. Z. Podowski, Prediction and analysis of onset of turbulent convective heat transfer deterioration in supercritical water flows, in: Proc. ICAPP 7, 2007.

[5] K. Yamagata, K. Nishikawa, S. Hasegawa, T. Fujii, S. Yoshida, Forced convective heat transfer to supercritical water flowing in tubes, Int. J. Heat Mass Transfer 15 (1972) 2575–2593.

[6] T. Gallaway, S. P. Antal, M. Z. Podowski, Multidimensional model of fluid flow and heat transfer in generation-iv supercritical water reactors, Nucl. Eng. Des. 238 (2008) 1909–1916.

[7] T. Gallaway, S. Antal, M. Z. Podowski, On the multidimensional modeling of fluid flow and heat transfer in scwrs, in: Proc. ICAPP'12, 2012, pp. 231–239.

[8] S. P. Antal, NPHASE-CMFD User Manual, Interphase Dynamics, LLC (2011).

[9] H. Kim, Y. Y. Bae, H. Y. Kim, J. H. Song, B. H. Cho, Experimental investigation on the heat transfer characteristics in a vertical upward flow of supercritical co2, in: Proc. of ICAPP, 2006.

[10] M. Z. Podowski, Thermal-hydraulic aspects of scwr design, Journal of Power and Energy Systems 2 (1) (2008) 352–360.